# Oxygen Vacancy Ordering in the Double-layered Ruddlesden−Popper Cobaltite $Sm_2BaCo_2O_{7-\delta}$

Lisa J. Gillie,*[,†,§] Joke Hadermann,[‡,§] Maryvonne Hervieu,[§] Antoine Maignan,[§] and Christine Martin[§]

*Department of Chemical & Biological Sciences, School of Applied Sciences, University of Huddersfield, Queensgate, Huddersfield HD1 3HD, United Kingdom, EMAT, University of Antwerp, Groenenborgerlaan 171, 2020 Antwerp, Belgium, and Laboratoire CRISMAT, ISMRA-ENSICAEN, 6 boulevard du Maréchal Juin, 14050 Caen cédex, France*

*Received April 10, 2008. Revised Manuscript Received July 30, 2008*

A new oxygen-deficient Ruddlesden−Popper (RP) cobaltite $Sm_2BaCo_2O_{7-\delta}$ ($\delta \approx 1.0$) has been synthesized and the crystal structure elucidated by Rietveld analysis of X-ray powder diffraction (XRD) data and transmission electron microscopy (TEM). The phase crystallizes in a primitive orthorhombic unit cell, with lattice parameters $a = 5.4371(4)$ Å; $b = 5.4405(4)$ Å and $c = 19.8629(6)$ Å, and space group *Pnnm*. Contrary to other oxygen-deficient cobalt RP phases, the oxygen vacancies are located in the equatorial positions of the [CoO] layers to give an intralayer structure similar to $Sr_2Mn_2O_5$, which is not usually observed for cobalt-containing materials. The $Sm^{3+}$ and $Ba^{2+}$ cations show a strong preference for distinct sites, with the majority of the larger $Ba^{2+}$ cations situated in the perovskite block layers and $Sm^{3+}$ cations predominantly in the rock salt layers. Magnetic susceptibility data demonstrate the strong antiferromagnetic (AFM) character of $Sm_2BaCo_2O_{7-\delta}$.

## Introduction

Cobalt-based perovskite materials have recently become interesting candidates for scientific investigation since it was discovered that they, like the Manganite perovskites, could exhibit magnetoresistance and charge-ordering effects.[1−4] Other remarkable physical phenomena such as thermoelectric and catalytic properties have also been observed in more complex crystal structures of cobalt-containing materials.[5−7] The flexibility of the cobalt oxidation state permits the manipulation of co-ordination environment, and hence structural type, therefore resulting in a broad spectrum of physical properties.

Materials containing cobalt in oxidation states ranging from univalent to tetravalent have been reported in oxide phases in the solid state. These range from the hydride reduced layered $LaSrCoO_{3.5-x}$ reported by Rosseinsky et al.,[8] which comprises of $Co^+$ and $Co^{2+}$ ions in a mixture of 4-, 5-, and 6-fold co-ordination, to the $Co^{4+}$-rich layered phases synthesized by Bréard and co-workers.[9] The more common cobalt valencies of $Co^{2+}$ and $Co^{3+}$ can be found in examples of perovskite and layered intergrowth Ruddlesden−Popper (RP) structural variants, wherein octahedral, and occasionally square-pyramidal, co-ordination is preferred; the brownmillerite $Sr_2Co_2O_5$ is built up of alternating octahedral and tetrahedral layers of trivalent metal cations;[10,11] trigonal prismatic geometry of $Co^{3+}$ is observed in the chain like structures of the $Ca_3Co_2O_6$ family of oxides.[12,13]

The so-called 112-type phases, $LnBaCo_2O_5$ and $LnBaCo_2O_{5+x}$ ($0 \leq x \leq 1$; dependent on $Ln^{3+}$) have attracted much interest over the past decade because of the significant magnetoresistance properties exhibited for some lanthanide species, this is the highest magnetoresistance ratio, $R_0/R_H < 10$, observed to-date in cobalt perovskite-based materials.[14−16] Some of the oxygenated forms of the 112 series can also give rise to spin-state transitions and a variety of superstructures.[17−20] The issue of trivalent cobalt, and the unusual spin multiplicities that can arise, has triggered great debate in the scientific literature. The intermediate spin-state, as explained by Demazeau et al. in 1979 for the $K_2NiF_4$-type phase

* Corresponding author. E-mail: L.J.Gillie@hud.ac.uk. Tel: 44 1482 472578. Fax: 44 1484 472182.
† University of Huddersfield.
§ Laboratoire CRISMAT, ISMRA-ENSICAEN.
‡ University of Antwerp.

(1) Jonker, G. H.; van Santen, J. H. *Physica* **1953**, *19*, 120.
(2) Briceno, G.; Chang, H.; Sun, X.; Schultz, P. G.; Xiang, X. D. *Science* **1995**, *270*, 273.
(3) Maignan, A.; Martin, C.; Hervieu, M.; Raveau, B. *J. Magn. Magn. Mater.* **2000**, *211*, 173.
(4) Maignan, A.; Martin, C.; Pelloquin, D.; Nguyen, N.; Raveau, B. *J. Solid State Chem.* **1999**, *142*, 247.
(5) Maignan, A.; Hébert, S.; Pi, L.; Pelloquin, D.; Martin, C.; Michel, C.; Hervieu, M.; Raveau, B. *Cryst. Eng.* **2002**, *5*, 365.
(6) Boullay, Ph.; Domengès, B.; Hervieu, M.; Groult, D.; Raveau, B. *Chem. Mater.* **1996**, *8*, 1482.
(7) Carberry, J. J.; Rajadurai, S.; Alcock, C. B.; Li, B. *Catal. Lett.* **1990**, *4*, 43.
(8) Hayward, M. A.; Rosseinsky, M. J. *Chem. Mater.* **2000**, *12*, 2182.
(9) Bréard, Y.; Michel, C.; Maignan, A.; Raveau, B. *Solid State Commun.* **2001**, *118*, 517.
(10) Grenier, J.-C.; Ghodbane, S.; Demazeau, G.; Pouchard, M.; Hagenmuller, P. *Mater. Res. Bull.* **1979**, *14*, 831.
(11) Rodríguez, J.; González-Calbet, J. M. *Mater. Res. Bull.* **1986**, *21*, 429.
(12) Hansteen, O. H.; Fjellvåg, H.; Hauback, B. C. *J. Mater. Chem.* **1998**, *8*, 2089.
(13) Hansteen, O. H.; Fjellvåg, H.; Hauback, B. C. *J. Mater. Chem.* **1998**, *8*, 2081.
(14) Zhou, W.; Lian, C. T.; Liang, W. Y. *Adv. Mater.* **1993**, *5*, 735.
(15) Fauth, F.; Suard, E.; Caignaert, V.; Domengès, B.; Mirebeau, I.; Keller, I. *Eur. Phys. J.* **2001**, *B21*, 163.
(16) Martin, C.; Maignan, A.; Pelloquin, D.; Nguyen, N.; Raveau, B. *Appl. Phys. Lett.* **1997**, *71*, 1421.

10.1021/cm8010138 CCC: $40.75 
Published on Web 09/13/2008

$La_2Li_{0.5}Co_{0.5}O_4$, has been reported to be present in several perovskite-based materials.[21,22]

Oxygen-deficient phases have been previously investigated for the double-layered $n = 2$ RP series ($A_{n+1}B_nO_{3n+1}$) by the groups of Cava and Weller.[23,24] $Sr_2Y_{1-x}Ca_xCo_2O_{6-y}$ ($0.2 \leq x \leq 0.5$ and $0 \leq y \leq 0.24$) has a cobalt valence state that varies from +2.36 to +2.75 due to a wide cation and anion homogeneity range. A body-centered tetragonal (*I*4/*mmm*; $a = 3.82765(6)$ Å; $c = 19.5795(3)$ Å) cell is observed for $Sr_2Y_{0.8}Ca_{0.2}Co_2O_6$, in which the apical oxygen anions linking the two perovskite layers along the [001] direction of the unit-cell are removed.[23] $Sr_3Co_2O_{7-x}$ ($0.94 \leq x \leq 1.22$) undergoes a reduction in symmetry from *I*4/*mmm* for $Sr_3Co_2O_{6.06}$ to *Immm* for an oxygen content of 5.94 per formula unit. The orthorhombic unit-cell arises due to the ordering of the oxygen vacancies which leads to a tripling of the *b*-parameter. In both cases square-pyramidal coordination is exhibited for the $Co^{3+}$, with the vacancies located in the apical positions of the perovskite blocks similar to the 112 phases.[24]

$Sm_2BaCo_2O_7$ was investigated by Siwen et al. in 1995; however, no detailed structural analysis was performed. It is claimed to be isostructural with $Sr_3Ti_2O_7$, displaying orthorhombic symmetry ($a = 3.821$Å; $b = 3.776$Å and $c = 19.426$Å). X-ray photoelectron spectroscopy (XPS) data suggest that the cobalt exists in a trivalent oxidation state, thus confirming an oxygen content of 7 per formula unit.[25,26]

Our studies have led us to believe that an oxygen-deficient phase, of nominal composition $Sm_2BaCo_2O_{7-\delta}$ ($\delta \approx 1.0$) can be synthesized, and this compound has been structurally characterized by Rietveld analysis of XRD data in combination with a transmission electron microscopy study. The ordering pattern proposed is interesting because of it seemingly being unique to this particular cobalt-based perovskite related material, hence giving an unusual example of a cobaltite with both an anion ordered lattice and a strong preference of the A-site cations for particular crystallographic sites.

## Experimental Section

Samples of $Sm_2BaCo_2O_{7-\delta}$ were synthesized by two different methods. First, by standard ceramic techniques using high purity metal oxides and carbonates as precursors, which were ground together in an agate mortar, followed by prolonged annealing in flowing oxygen at 1100 °C. This afforded a black powder which was highly crystalline but was composed of two distinct phases; an oxygenated 112-type phase $SmBaCo_2O_{5+x}$ ($x \approx 0.5$), and the double-layered RP target compound. A single phase sample was unable to be obtained via this method under these conditions. Alternatively, using an initial composition of $Sm_2BaCo_2O_{7.5}$ from the appropriate quantities of $Sm_2O_3$, $BaO_2$, Co, and $Co_3O_4$, the finely ground precursor powder, contained in an alumina finger, could be sealed in an evacuated silica tube and heated to 1075 °C for a period of 48 h before cooling slowly to ambient temperature. This also resulted in an $n = 2$ RP material, but with poorer crystallinity and peak shape for the XRD profile than that observed for the oxygen annealed sample. Because it was not possible to definitively exclude the presence of the oxygenated 112 phase due to the broad peak shape, only the oxygen annealed sample was considered in this paper.

Electron diffraction (ED) patterns and high-resolution electron microscopy (HREM) images were recorded on JEOL 2010 EX and TOPCON 002B (200 kV, 1.8 Å point resolution) microscopes respectively, equipped with an EDS (energy-dispersive spectroscopy) analyzer. The specimens for microscopy were prepared by crushing the crystals in butanol and depositing them on a holey carbon film. Theoretical HREM images were calculated using the MacTempas software package.

Rietveld refinement using the General Structure Analysis System (GSAS package)[27] was performed on XRD data collected on a Philips vertical diffractometer with Cu Kα radiation. Magnetization data were collected on Quantum Design magnetometers. Temperature dependent data were recorded in an applied field of 100 Gauss in both zero-field cooled (zfc) and field-cooled (fc) modes, from 5 to 400 K. The magnetization curve [M(H)] was measured up to 14 T at 10 K. For the higher temperatures (i.e., from 300 to 800 K) the magnetic susceptibility data were obtained by using a Faraday balance with a field of 3000 Gauss.

## Results and Discussion

The compositions of the component phases in the oxygen annealed sample were investigated by EDS-TEM studies, and this provided a starting model for the structural refinements. The 112 structure was included as a secondary phase in the refinements.

The electron diffraction investigation confirms the presence of two phases as observed by XRD. EDS analyses were performed on both phases, and showed the cationic compositions $Sm_{1.99 \pm 0.06}Ba_{0.67 \pm 0.02}Co_{2.00 \pm 0.04}$ and $Sm_{0.96 \pm 0.04}Ba_{0.96 \pm 0.06}Co_{2.00 \pm 0.05}$. To confirm that the latter phase is $SmBaCo_2O_{5+x}$, we made a series of electron diffraction patterns and reconstructed the reciprocal lattice. This showed cell parameters close to those reported in literature and the reflection conditions were also in agreement, further supporting the conclusion that the second phase is $SmBaCo_2O_{5+x}$.[14−20] The composition of the main $n = 2$ RP phase will be addressed in more detail shortly.

The electron diffraction patterns for the main phase are shown in Figure 1. They can be indexed using lattice parameters $a \approx b \approx 5.4$ Å ($\sim 2a_p$, where $a_p$ is the basic perovskite subcell parameter) and $c \approx 19.4$ Å. The *c* parameter is close to those known for various double-layered RP-type phases. The reflection conditions that were derived

(17) Akahoshi, D.; Ueda, Y. *J. Phys. Soc. Jpn.* **1999**, *68*, 736.
(18) Suard, E.; Fauth, F.; Caignaert, V.; Mirebeau, I.; Baldinozzi, G. *Phys. Rev. B.* **2000**, *6*, 1–R11871.
(19) Frontera, C.; García-Muñoz, J. L.; Llobet, A.; Aranda, M. A. G. *Phys. Rev. B.* **2002**, *65*, 180405(R)
(20) Anderson, P. S.; Kirk, C. A.; Knudsen, J.; Reaney, I. M.; West, A. R. *Solid State Sci.* **2005**, *7*, 1149.
(21) Demazeau, G.; Courbin, Ph.; Le Flem, G.; Pouchard, M.; Hagenmuller, P.; Soubeyroux, J.-L.; Main, I. G.; Robins, G. A. *Nouv. J. Chim.* **1979**, *3*, 171.
(22) Demazeau, G.; Pouchard, M.; Thomas, M.; Colombet, J.-F.; Grenier, J.-C.; Fournés, L.; Soubeyroux, J.-L.; Hagenmuller, P. *Mater. Res. Bull.* **1980**, *15*, 451.
(23) Yamaura, K.; Huang, Q.; Cava, R. J. *J. Solid State Chem.* **1999**, *146*, 277.
(24) Dann, S. E.; Weller, M. T. *J. Solid State Chem.* **1992**, *97*, 179.
(25) Siwen, L.; Yufang, R. *Mater. Res. Bull.* **1994**, *29*, 993.
(26) Siwen, L.; Yufang, R. *J. Solid State Chem.* **1995**, *114*, 286.
(27) Larson, A. C.; Von Dreele, R. B. *General Structural Analysis System (GSAS)*; Report LAUR 86-748; Los Alamos National Laboratory: Los Alamos, NM, 2000.

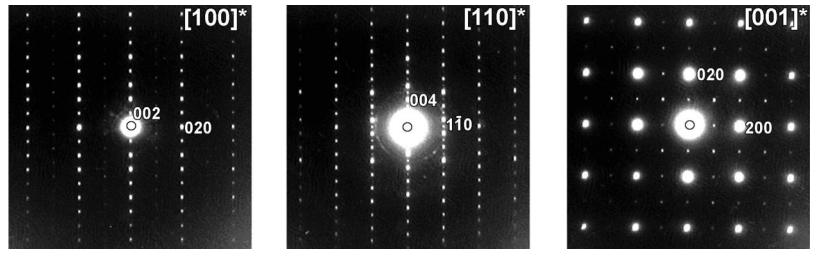


**Figure 1.** Electron diffraction patterns of $Sm_2BaCo_2O_{7-\delta}$ along the three main zones [100], [110], and [001].

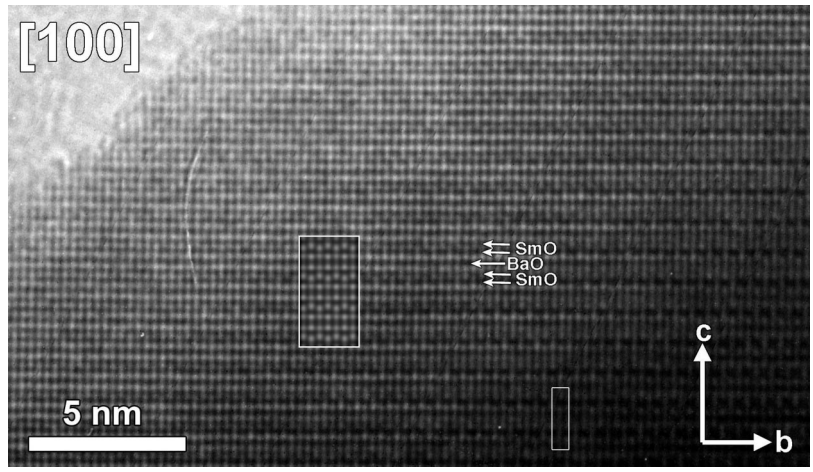


**Figure 2.** High-resolution electron microscopy image of $Sm_2BaCo_2O_{7-\delta}$ along the [100] direction. One unit cell in projection is indicated by a white rectangle, the simulation is marked by a white border. The SmO and BaO layers are indicated by arrows. The black dots in these rows correspond to the cations.

from the electron diffraction patterns are *hk*0, no conditions; 0*kl*, $k + l = 2n$; *h*0*l*, $h + l = 2n$; *hhl*, no extinctions; *h*00, $h = 2n$; 0*k*0, $k = 2n$; 00*l*, $l = 2n$. These reflection conditions are in agreement with two extinction symbols, the tetragonal *P-n-* and the orthorhombic *Pnn-*. To decide between these two possibilities, a difference in length between the cell parameters *a* and *b* would be sufficient. All measurements done on the electron diffraction patterns fail to evidence such difference. However, the precision of cell parameters determined from measurements of electron diffraction patterns is rather low, typically ±0.1 Å. Thus, a final conclusion about the structure being tetragonal or orthorhombic cannot be made at this point and has to be done during the XRD refinements. This leaves as possible space groups in agreement with the electron diffraction patterns, the orthorhombic space groups *Pnnm* and *Pnn*2, and the tetragonal space groups $P4_2nm$, $P\bar{4}n2$, and $P4_2/mnm$.

High-resolution electron microscopy images along the [100], [110], and [001] directions are shown in Figures 2−4, respectively. In the [100] and [110] images, the Sm atom columns and the Ba atom columns are projected as black dots in the rows indicated by the arrows, on the [001] image the cation columns are projected as the white dots. On the [100] image the periodicity of 5.4 Å is clearly visible along the *b*-axis in the thicker part of the crystal (right side of the image) as an alternation of black and white regions. In the thinner part this periodicity is observed in the double $Sm_2O_2$ layers (indicated by arrows) as a slight zigzag ordering of the bright dots in these layers. The [110] image shows that the layer-stacking is the same as for an $n = 2$ RP-type

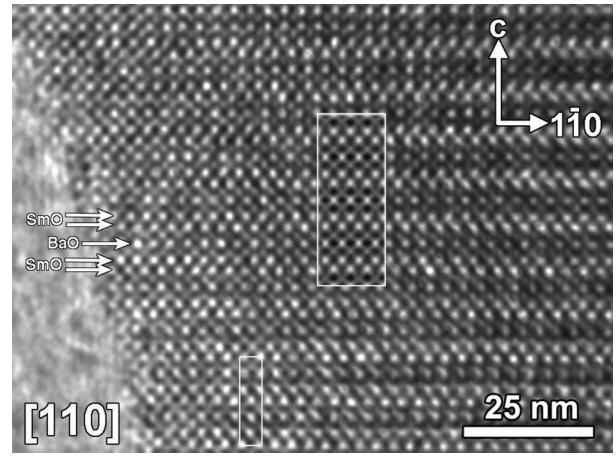


**Figure 3.** High-resolution electron microscopy image of $Sm_2BaCo_2O_{7-\delta}$ along the [110] direction. The simulated image is marked by a white border, with the dimensions of one unit cell in projection indicated by a white rectangle. The SmO and BaO layers are indicated by arrows. The black dots in these rows correspond to the cations.

structure.[28] On the [001] image no clear difference with the characteristic $a_p \times a_p$ ($a_p$ =basic perovskite subcell parameter) can be seen by eye, however, when performing a Fourier transform, a clear $2a_p \times 2a_p$ superstructure is observed, in agreement with the diffraction patterns shown in Figure 1.

The Rietveld refinement of the XRD data was first carried out using the tetragonal space-group $P4_2/mnm$ with the model

(28) Hadermann, J.; Van Tendeloo, G.; Abakumov, A. M. *Acta Crystallogr., Sect. A* **2005**, *61*, 77.

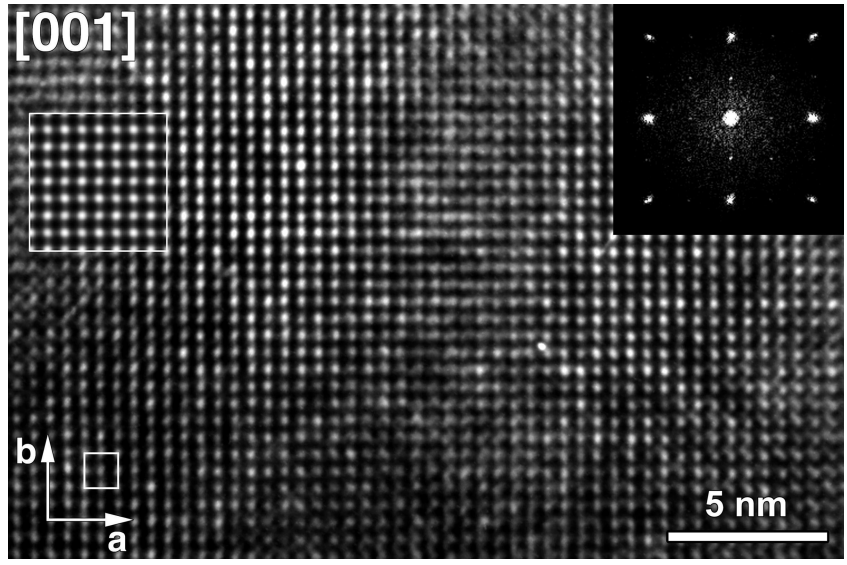


**Figure 4.** High-resolution electron microscopy image of $Sm_2BaCo_2O_{7-\delta}$ along the [001] direction. The simulated image is marked by a white border, with the dimensions of one unit cell in projection indicated by a white rectangle. The cation columns are projected as the white dots. The Fourier transform of the image is inserted in the top right corner to give evidence for the presence of the $2a_p$ superstructure present in the $a-b$ plane.

used by Battle et al.[29] for $HoSr_2Mn_2O_7$, in which the lanthanide and alkaline-earth cations were distributed over two distinct mixed sites: 44% of Ho in the rock salt layers (*8*j) and 12% of Ho in the perovskite layers (*4*f). In agreement with these results and others dealing with 112 phases, the starting model was built with the larger ($Ba^{2+}$) and smaller ($Sm^{3+}$) cations perfectly ordered in the perovskite and rock salt layers, respectively. Then, the agreement between calculated and experimental profiles was improved somewhat upon the introduction of a slight orthorhombic distortion and the use of the *Pnnm* space-group (R-factors for tetragonal space group <20%). This leads to very similar lattice parameters ($a = 5.4371(4)$ Å and $b = 5.4405(4)$ Å) that cannot be distinguished one from the other by microscopy. To give an estimate of what it is possible to distinguish: using the camera constant as used for the presented electron diffraction patterns (19 mm Å), this difference of 0.0034 Å would require a row of 227 reflections along this direction before a spot splitting of half a millimeter would be visible. The electron diffraction patterns for the [001] zone of the current sample usually show only up to 12 reflections in a row along *a* and *b*, thus giving the possibility only to observe (half a millimeter) spot splitting due to orthorhombicity for differences between *a* and *b* starting from approximately 0.06 Å. At this stage, the extra reflections in the XRD profile due to the parasite phase, the oxygenated 112 phase whose presence was also confirmed by the microscopy studies, could be observed. The refinement was then modified to include this second phase and a full structural refinement was carried out on both phases present in the sample when both the oxygen vacancy ordering and A-site cation ordering were considered.

In fact, although XRD is not the ideal method for the detection of oxygen anions, because of its relative insensitivity to light elements, it can provide an idea of the occupation of atomic sites. Neutron diffraction also would not be ideal for this sample because of the large neutronic absorption of the $^{62}Sm$ isotope; it would be necessary to prepare samples using a different isotope of Sm to gain insightful information from neutron diffraction experiments. This is also not ideal for this sample because of the difficulty in attaining larger quantities of the well-crystallized product from syntheses with only average reproducibility. The refinement was performed with the aim of locating any preference of crystallographic site for the oxygen vacancies and to give a rough idea of the concentration. The fractional occupancies of the oxygen sites were therefore allowed to vary while the thermal agitation parameters were constrained to sensible values. Only one site appeared to be less than full when all of the oxygen fractional occupancies were allowed to refine indiscriminately; this was the O3 (4*f*) position, which was stable with a maximum occupation of ca. 7%. Because the O(3) fractional occupancy was so low, this site was subsequently fixed to have a fractional occupancy of zero. Upon careful inspection of the XRD pattern, it could be seen that emptying this oxygen site improved the fit without ambiguity, and there is a particularly strong effect on the intensity of the 101/011 Bragg peaks (at about 17° in $2\theta$). All other O-sites were therefore assumed to be 100% filled, because the refinement began to diverge if other oxygen positions were forced to accept any vacancies. If we consider this one particular oxygen site to be almost completely vacant, then this gives rise to an interesting defect structure in the double perovskite block layers leading to the reduction of octahedrally coordinated $Co^{3+}$ in the stoichiometric $n = 2$ RP structure ($O_7$) to a phase where the large majority of transition metal cations exist as $Co^{2+}$ in a square-pyramidal geometry. Contrary to what is generally seen for RP Cobalt-based materials, the vacancies are all in the equatorial positions of the perovskite layers, thus leading to an intralayer vacancy ordered structure similar to that seen in $Sr_2Mn_2O_5$.[30] The ordering on the perovskite block layers can be described

(29) Battle, P. D.; Millburn, J. E.; Rosseinsky, M. J.; Spring, L. E.; Vente, J. F. *Chem. Mater.* **1997**, *9*, 3136.

as the linking, via vertices of pairs of square-based pyramidal $CoO_5$ units, to yield sheets in which six-sided holes are formed, refer to Figure 5a. The pattern of the neighboring layer in the double perovskite sheet can be viewed as being rotated at an angle of 90° to the adjoined sheet. This can be seen more clearly in panels b and c in Figure 5. Other evidence which points to the oxygen vacancy ordering scheme proposed is the presence of two different Co−Co bond lengths in the structure; one of 3.96 and one of 3.73 Å. The longer bond length links two cobalt ions via a filled oxygen site, whereas the shorter bond length links two cobalt ions in a perovskite layer via the vacant O(3) site.

The last point deals with the actual cationic composition and preference of the A-site cations for particular sites. In fact the EDS analysis leads to a formula close to $Sm_2Ba_{0.7}Co_2$, but no evidence of Ba deficiency is observed on the 4*g* site; the refinement suggests that all cationic sites are completely filled. The other possibility is that the composition is not exactly as expected, because of the presence of a second phase, and therefore we must consider other combinations of the three component cations that may account for the discrepancy between the EDS and refinement results. It should also be noted that the associated error of both of these methods is ca. 5%, hence it is difficult in this case to state a definitive composition. The composition is thus probably better described by the EDS formula $Sm_{2.13}Ba_{0.75}Co_{2.12}$. $Ba^{2+}$ and $Sm^{3+}$ have similar contrast for X-rays ($54e^-$ and $59e^-$) and it is therefore difficult to determine the distribution of the cations over the 4*g* and 8*h* sites. Several distributions were successively tried. The repartition of the cations is probably close to $Ba_{0.75}Sm_{0.25}$ in the perovskite layer, with the remaining cations ($Sm_{0.94}Co_{0.06}$) lying in the rock salt layer that is susceptible to accommodate several kinds of cations.[31] The refinement was first performed using the ideal cation composition $Sm_2BaCo_2$ and it proceeded smoothly and converged with $\chi^2 = 1.651$ and agreement factors $R_p = 10.21\%$ and $R_{wp} = 13.92\%$ (*Pnnm*; $a = 5.4317(4)$ Å; $b = 5.4405(4)$ Å; $c = 19.8629(6)$ Å) with the oxygenated 112-type phase included as a parasite phase (*Pmmm*; $a = 3.8899(2)$ Å; $b = 7.7985(4)$ Å; $c = 7.5858(3)$ Å; 5 wt %). A second refinement was then performed with the nonideal composition represented by the EDS formula $Sm_{2.13}Ba_{0.75}Co_{2.12}$, with the cationic distribution as discussed previously. This resulted in a very minor improvement to the refinement statistics ($\chi^2 = 1.643$ and agreement factors $R_p = 10.26\%$ and $R_{wp} = 13.91\%$); however, this could be viewed as being insignificant as very similar results could be attained using slight variations on the composition, within the 5% error limit. For completeness, a two phase refinement was also performed which allowed the fractional occupancies of the A-site cations to vary over the 4*g* and 8*h* sites. The ideal A-site composition of $Sm_2Ba$ was used as a starting model for simplicity, and the refinement converged with almost identical statistics to the ordered model ($\chi^2 = 1.649$ and agreement factors $R_p = 10.22\%$ and $R_{wp} = 13.91\%$; 4*g* site occupancies Ba 0.76(6)/Sm 0.24(6); 8*h* occupancies Ba

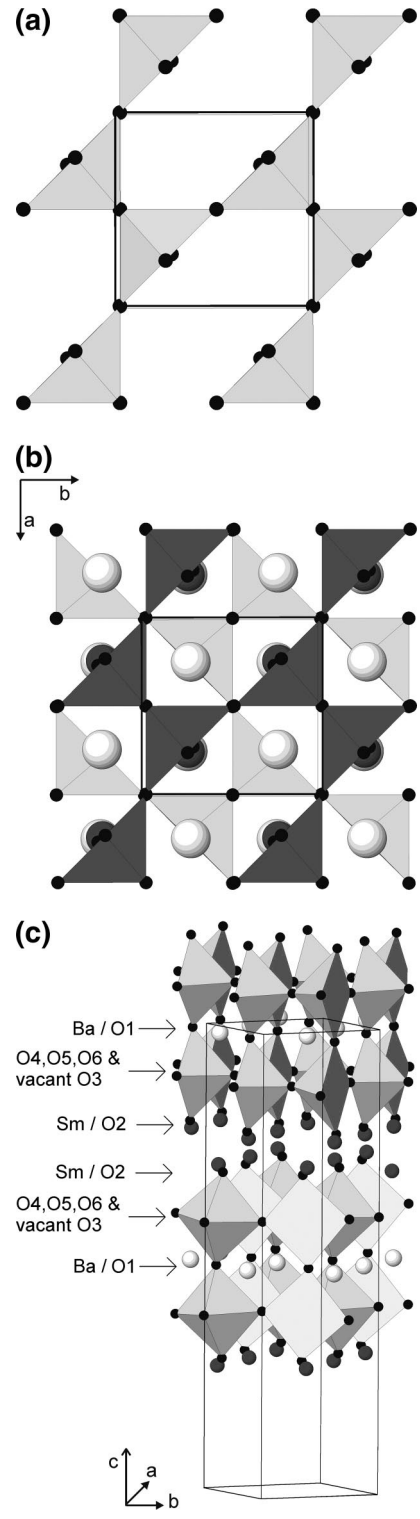


**Figure 5.** (a) View down the [001] direction of the unit-cell showing the ordering of oxygen vacancies in a single sheet of the double perovskite block. Grey polyhedra are $CoO_5$ units and the black spheres are oxygen anions. The solid black line represents the unit-cell perimeter. (b) View onto the (*a*, *b*) basal plane of $Sm_2BaCo_2O_{7-\delta}$. Dark polyhedra are upper layer of $CoO_5$ units in double perovskite block; light polyhedra are lower layer of $CoO_5$ units in double perovskite block; black spheres are oxygen anions; light gray spheres are $Ba^{2+}$ cations and dark gray spheres are $Sm^{3+}$ cations. Solid black line represents the unit-cell perimeter. (c) View of the three-dimensional structure, showing the $CoO_5$ pyramids in the perovskite blocks; black spheres are oxygen anions; light gray spheres are $Ba^{2+}$ cations and dark gray spheres are $Sm^{3+}$ cations. The horizontal arrows indicate the vacant O(3) sites and the elongated Co−O(2) bond distances.

(30) Caignaert, V. *J. Magn. Magn. Mat.* **1997**, *166*, 117.
(31) Maignan, A.; Hébert, S.; Hervieu, M.; Michel, C.; Pelloquin, D.; Khomskii, D. *J. Phys.: Condens. Matter* **2003**, *15*, 2711.

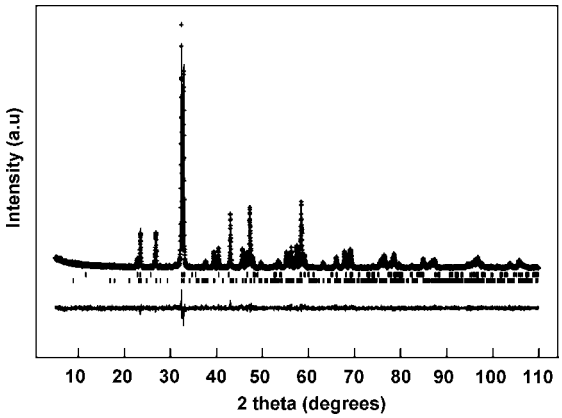


**Figure 6.** Calculated, experimental (+), and difference (−) profiles for Rietveld refinement of XRD data for $Sm_2BaCo_2O_{7-\delta}$ ($\delta \approx 1.0$). The lower tick marks represent the reflection positions for the primary phase and the upper ones represent those for the parasite phase.

**Table 1. Refined Parameters and Refined Interatomic Distances of $Sm_2BaCo_2O_{7-\delta}$[a]**

| type | site | *x* | *y* | *z* | $U_i/U_e$*100 (Å$^2$) | fractn. |
|---|---|---|---|---|---|---|
| Ba | 4*g* | 0.754(3) | 0.251(2) | 0.5 | 0.43(9) | 1.0 |
| Sm | 8*h* | 0.757(2) | 0.238(1) | 0.682(1) | 0.39(6) | 1.0 |
| Co | 8*h* | 0.760(4) | 0.255(3) | 0.902(2) | 0.56(1) | 1.0 |
| O(1) | 4*g* | 0.755(3) | 0.741(2) | 0.5 | 1.0 | 1.0 |
| O(2) | 8*h* | 0.759(1) | 0.288(7) | 0.792(1) | 1.0 | 1.0 |
| O(3) | 4*f* | 0.5 | 0 | 0.023 | 0.0[b] | 0.0[b] |
| O(4) | 4*f* | 0.5 | 0 | 0.107(4) | 1.0 | 1.0 |
| O(5) | 4*e* | 0.5 | 0.5 | 0.607(6) | 1.0 | 1.0 |
| O(6) | 4*e* | 0.5 | 0.5 | 0.894(5) | 1.0 | 1.0 |

Metal−Oxygen Bond Lengths (Å)

| | | | | | | |
|---|---|---|---|---|---|---|
| Co−O(1) | 1.96(1) | Sm−O(2) | 2.21(2) | Ba−O(1) | 2.78(8) | |
| Co−O(2) | 2.18(2) | Sm−O(2) | 2.72(6) | Ba−O(1) | 2.66(8) | |
| Co−O(4) | 1.98(2) | Sm−O(2) | 2.51(4) | Ba−O(1) | 2.77(13) | |
| Co−O(5) | 1.91(2) | Sm−O(2) | 3.04(4) | Ba−O(1) | 2.67(13) | |
| Co−O(6) | 1.95(2) | Sm−O(4) | 2.44(5) | Ba−O(4) | 2.86(6) | (×2) |
| | | Sm−O(5) | 2.49(6) | Ba−O(5) | 2.87(8) | (×2) |
| | | Sm−O(6) | 2.38(5) | Ba−O(6) | 2.84(6) | (×2) |

[a] Oxygen thermal parameters were constrained to a sensible value and not refined. *Pnnm*; $a = 5.4371(4)$ Å, $b = 5.4405(4)$ Å, and $c = 19.8629(6)$ Å; $\chi^2 = 1.651$; $R_{wp} = 13.92\%$ and $R_p = 10.91\%$. [b] * denotes O(3) site where the fractional occupancy, and hence thermal parameter, were fixed to zero.

0.12(3)/Sm 0.88(3)). There is no significant difference between the refinements for the ordered and disordered models and therefore it can only be inferred that there is a strong preference for the $Sm^{3+}$ and $Ba^{2+}$ cations to occupy the rocksalt and perovskite layers, respectively. It should be noted that we have confidence in the refinement model used; however, the main problem lies with the difficulty in producing high-quality crystalline samples of this material, even though this particular sample is of superior quality to the only related phase reported to-date in the scientific literature.[25,26] It can only be concluded that with the constituent elements in this phase, and the techniques available, it is virtually impossible to distinguish between the A-site cations and elucidate an exact distribution; hence, for clarity, this phase will be described as having the nominal composition $Sm_2BaCo_2O_{7-\delta}$ throughout this paper. The refinement results presented are those for the ideal ordered composition. The refinement profile is depicted in Figure 6, with the refined parameters detailed in Table 1.

It can be noted that the Co−O(2) distances are longer than the other Co−O bond lengths (Figure 5c). These correspond to the apical oxygens that are located at the extremities of the double perovskite block, in close proximity to the majority of the $Sm^{3+}$ cations. It is possible that an electrostatic attraction between these two high charge density ions is responsible for this distortion of the Co−O(2) bond length, in comparison to the other metal−oxygen distances. The opposite effect is seen in $n = 2$ RP staged oxyfluoride phases such as $La_{1.2}Sr_{1.8}Mn_2O_7F$, where $F^-$ anions are intercalated into alternate rock salt layers. This results in a significant shortening in length of the Mn−O bonds adjacent to the intercalated fluorine, which can be satisfactorily explained by the consideration of the electrostatic attractions and repulsions between the Mn cations and $F^-$ cations, and the $O^{2-}$ and $F^-$ cations.[32,33]

Results presented by Siwen et al. for the oxygenated parent material $Sm_2BaCo_2O_7$ state that orthorhombic symmetry is exhibited, and also that the oxygen content is 7 per formula unit, giving rise to a pure trivalent Co oxidation state. Because their XRD data are not refined to establish the structure, it is difficult to judge of the quality of their samples and to compare with our samples. Nevertheless our refined cell parameters can be compared to an equivalent of those previously reported with a simple perovskite subcell by multiplying by a factor of $\sqrt{2}$ for *a* and *b*; this would give rise to supercell lattice parameters of $a = 5.404$ Å, $b = 5.340$ Å, and $c = 19.426$ Å.[25,26] These are significantly reduced compared to the lattice parameters suggested by our Rietveld refinement, which is therefore consistent with a change in size of the transition metal cation (i.e., in Co valence), and consequently in oxygen content.

Techniques such as XANES or ELNES could be interesting tools to confirm this model via the determination of the Co oxidation state (which is expected to be close to 2).

The refined structure is supported by Figures 2−4, which show HREM observed and calculated images along the [100], [110], and [001] directions, respectively. The refined structure was used as input for calculating the simulated images, which are marked by a white border on the experimental images. For Figure 2, the best agreement was achieved for defocus value $\Delta f = -150$ Å and thickness $t = 24$ Å. For Figure 3, a defocus value of $\Delta f = -520$ Å and thickness of $t = 32$ Å allowed a picture to be taken that was easily comparable with the structure. As mentioned previously, at both defocus values the Sm atom columns and the Ba atom columns are projected as black dots in the rows indicated by the arrows. Figure 4 could be best reproduced using a defocus value of $\Delta f = -260$ Å and a thickness of $t = 40$ Å. On the calculated image for the [100] direction one can clearly recognize the zigzag pattern of the bright dots in the $Sm_2O_2$ double layers which is also present on the experimental image. This zigzag is due to the variation in distance along the *b*-axis between the projected columns of Sm atoms, alternating one short Sm column-column distance with one long one. This results in a bright dot in between the Sm columns where the columns are far apart, and the absence of such a dot where they are closer together. The calculated image for the [100] high-

(32) Aikens, L. D.; Gillie, L. J.; Li, R. K.; Greaves, C. *J. Mater. Chem.* **2001**, *12*, 264.
(33) Gillie, L. J., PhD Thesis, University of Birmingham, Birmingham, AL, 2003.

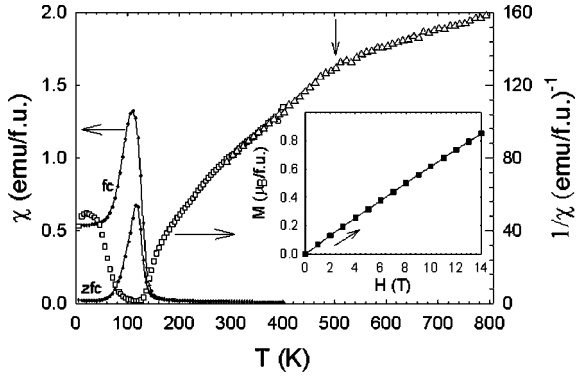


**Figure 7.** Susceptibility and inverse susceptibility curves, left and right *y*-axes, respectively; measured in 100 G for 4−400 K (SQUID) and in 3000 G for 300−800 K (Faraday balance). Inset shows magnetic field dependence of the magnetization at 10 K.

resolution image shows no superstructure visible to the eye, as is also the case for the experimental image; however, as for the experimental image, the Fourier transform does show the superstructure, in the same way the corresponding simulated diffraction pattern at this thickness (not shown) also shows the superstructure as seen on the experimental electron diffraction pattern of Figure 1. Thus along all three directions there is a good agreement between the experimental and calculated images.

## Magnetic Characterization

The data reported in Figure 7 show the strong antiferromagnetic character of $Sm_2BaCo_2O_{7-\delta}$. At 10K (inset of Figure 7) the magnetization value actually reaches only ~0.8 $\mu_B$ for one unit formula, i.e., two cobalt ions. The inverse susceptibility curve exhibits a break around 500K, indicated by the vertical arrow, and the extrapolation of the linear part (>470 K) leads to a large negative $\theta_p$ value. Unfortunately, due to the short temperature range of the linear part, and because of the existence of the secondary phase, it is not possible to extract reliable $\mu_{eff}$ values from these data that could give an estimation of the valence of Co. Thus neutron diffraction is needed, not only to know the precise crystal structure and the oxygen content, but also (vs temperature) to know if this characteristic temperature corresponds to a magnetic transition ($T_N$). Only a very small ferromagnetic component is observed in the susceptibility curve around 100K, whose origin is unclear, but which may be connected with a canting of the antiferromagnetism. In fact, it is unlikely to come from the parasitic impurity, the 112 phase, because of its small amount (5% in weight, or 7% in molar ratio) and its characteristic transition temperature range,[4] higher than 100 K observed here. It is clear that definitive conclusions dealing with the magnetic behavior of this compound are not feasible due to the quality of the sample (biphasic with a variable oxygen content), and the magnetic curves presented here are only to give a general survey of the magnetic background of this sample.

The 2D character of the structure is compatible with a strong antiferromagnetism; as for instance, the RP ($n = 2$) oxychloride $Sr_3FeCoO_5Cl_2$.[34]

## Summary

A new oxygen-deficient $n = 2$ RP cobaltite has been synthesized which exhibits both anion ordering and a strong preference of the A-site cations for particular positions within the structure. The larger $Ba^{2+}$ cations are preferentially situated in the perovskite block layers (4*g*) and the smaller $Sm^{3+}$ cations are located principally in the rock salt layers (8*h*). The precise cationic distribution and composition cannot be determined unequivocally due to the limitations of the techniques available; however, we have demonstrated that the differences in suggested composition from both bulk diffraction and EDS analyses could be explained by the similarities in X-ray scattering power of the $Sm^{3+}$ and $Ba^{2+}$ cations. However, it is possible, because a parasite phase is also present, that the actual composition may deviate slightly from that expected, and we propose that the true composition is probably close to $Sm_{2.1}Ba_{0.8}Co_{2.1}O_{7-\delta}$ (where $\delta \approx 1$). The anion vacancies appear to only affect one of the oxygen atomic positions and the O(3) 4*f* site is suggested to be almost completely empty, thus giving rise to a defect structure in which the intralayer ordering scheme is similar to that observed for $Sr_2Mn_2O_5$. Sheets of vertex-linked pairs of $CoO_5$ units with hexagonal holes are formed. Neighboring sheets in the double perovskite block layers are rotated 90° with respect to each other. This is contrary to the series of phases observed by Cava et al. wherein the vacancies affected the apical oxygen positions within the perovskite block layers. $Sm_2BaCo_2O_{7-\delta}$ has a strong antiferromagnetic character, but due to the biphasic nature of the sample more in-depth magnetic characterization of this phase is not currently feasible.

**Acknowledgment.** The authors thank Dr. N. Nguyen for magnetic measurements and the European Union for fellowships to L.J.G. and J.H. (SCOOTMO HRPN-CT-2002-00293 and SUPER-GMR HRPN-CT-2000-0021, respectively).

CM8010138

(34) Knee, C. S.; Field, M. A. L.; Weller, M. T. *Solid State Sci.* **2004**, *6*, 443.